2003

ep → ep π^0 Reaction Studied in the Δ(1232) Mass Region Using Polarization Asymmetries

M. Bektasoglu
Old Dominion University

L. Ciciani
Old Dominion University

K.V. Dharmawardane
Old Dominion University

G. E. Dodge
Old Dominion University, gdodge@odu.edu

T.A. Forest
Old Dominion University

See next page for additional authors

Original Publication Citation

Bektasoglu, M., Dharmawardane, K.V., Dodge, G.E., Hyde-Wright, C.E., Kuhn, S.E., Weinstein, L.B., et al., CLAS Collaboration (2003). ep → ep π^0 reaction studied in the Δ(1232) mass region using polarization asymmetries. *Physical Review C, 68*(3), 1-14, Article 035202. https://doi.org/10.1103/PhysRevC.68.035202

Authors
M. Bektasoglu, L. Ciciani, K.V. Dharmawardane, G. E. Dodge, T.A. Forest, C.E. Hyde-Wright, A. Klein, A. V. Klimenko, S. E. Kuhn, S. Stepanyan, L. B. Weinstein, et al., and CLAS Collaboration

$ep \rightarrow ep\pi^0$ reaction studied in the $\Delta(1232)$ mass region using polarization asymmetries

A. Biselli,[1,*] G. S. Adams,[1] M. J. Amaryan,[37] E. Anciant,[24] M. Anghinolfi,[13] B. Asavapibhop,[28] G. Asryan,[37] G. Audit,[24] T. Auger,[24] H. Avakian,[12] S. Barrow,[10] M. Battaglieri,[13] K. Beard,[16] M. Bektasoglu,[21] W. Bertozzi,[19] N. Bianchi,[12] S. Boiarinov,[14] B. E. Bonner,[23] P. Bosted,[28] S. Bouchigny,[17] R. Bradford,[3] D. Branford,[8] W. K. Brooks,[17] S. Bueltmann,[35] V. D. Burkert,[17] J. R. Calarco,[30] D. S. Carman,[22] B. Carnahan,[4] C. Cetina,[11] L. Ciciani,[21] P. L. Cole,[34] A. Coleman,[6] J. Connelly,[11] D. Cords,[17] P. Corvisiero,[13] D. Crabb,[35] H. Crannell,[4] J. Cummings,[1] E. De Sanctis,[12] R. De Vita,[13] P. V. Degtyarenko,[17] R. A. Demirchyan,[37] H. Denizli,[31] L. C. Dennis,[10] K. V. Dharmawardane,[21] K. S. Dhuga,[11] C. Djalali,[33] G. E. Dodge,[21] J. Domingo,[17] D. Doughty,[5,17] P. Dragovitsch,[10] M. Dugger,[2] S. Dytman,[31] M. Eckhause,[6] Y. V. Efremenko,[14] H. Egiyan,[6] K. S. Egiyan,[37] L. Elouadrhiri,[5,17] A. Empl,[1] P. Eugenio,[10] L. Farhi,[24] R. Fatemi,[35] R. J. Feuerbach,[3] J. Ficenec,[36] K. Fissum,[19] T. A. Forest,[21] A. Freyberger,[17] V. Frolov,[1] H. Funsten,[6] S. J. Gaff,[7] M. Gai,[27] G. Gavalian,[37] V. B. Gavrilov,[14] S. Gilad,[19] G. P. Gilfoyle,[32] K. L. Giovanetti,[16] P. Girard,[33] E. Golovatch,[29] K. A. Griffioen,[6] M. Guidal,[15] M. Guillo,[33] L. Guo,[17] V. Gyurjyan,[17] D. Hanock,[6] J. Hardie,[5] D. Heddle,[5,17] F. W. Hersman,[30] K. Hicks,[22] R. S. Hicks,[28] M. Holtrop,[30] J. Hu,[1] C. E. Hyde-Wright,[21] M. M. Ito,[17] D. Jenkins,[36] K. Joo,[35] J. H. Kelley,[7] M. Khandaker,[20,17] K. Y. Kim,[31] K. Kim,[18] W. Kim,[18] A. Klein,[21] F. J. Klein,[17] A. V. Klimenko,[21] M. Klusman,[1] M. Kossov,[14] L. H. Kramer,[9,17] Y. Kuang,[6] J. Kuhn,[1] S. E. Kuhn,[21] J. Lachniet,[3] J. M. Laget,[24] D. Lawrence,[28] G. A. Leksin,[14] A. Longhi,[4] K. Loukachine,[36] R. W. Major,[32] J. J. Manak,[17] C. Marchand,[24] S. K. Matthews,[4] S. McAleer,[10] J. W. C. McNabb,[3] J. McCarthy,[35] B. A. Mecking,[17] M. D. Mestayer,[17] C. A. Meyer,[3] R. Minehart,[35] M. Mirazita,[12] R. Miskimen,[28] V. Mokeev,[29] V. Muccifora,[12] J. Mueller,[31] L. Y. Murphy,[11] G. S. Mutchler,[23] J. Napolitano,[1] S. O. Nelson,[7] G. Niculescu,[22] B. Niczyporuk,[17] R. A. Niyazov,[21] M. Nozar,[17] J. T. O'Brien,[4] G. V. O'Rielly,[11] M. S. Ohandjanyan,[37] M. Osipenko,[29] K. Park,[18] Y. Patois,[33] G. A. Peterson,[28] S. Philips,[11] N. Pivnyuk,[14] D. Pocanic,[35] O. Pogorelko,[14] E. Polli,[12] B. M. Preedom,[33] J. W. Price,[26] L. M. Qin,[21] B. A. Raue,[9,17] G. Riccardi,[10] G. Ricco,[13] M. Ripani,[13] B. G. Ritchie,[2] S. Rock,[28] F. Ronchetti,[12] P. Rossi,[12] D. Rowntree,[19] P. D. Rubin,[32] K. Sabourov,[7] C. W. Salgado,[20] V. Sapunenko,[13] M. Sargsyan,[37] R. A. Schumacher,[3] V. S. Serov,[14] Y. G. Sharabian,[37] J. Shaw,[28] S. M. Shuvalov,[14] S. Simionatto,[11] A. Skabelin,[19] E. S. Smith,[17] L. C. Smith,[35] T. Smith,[30] D. I. Sober,[4] L. Sorrell,[28] M. Spraker,[7] S. Stepanyan,[37,21] P. Stoler,[1] I. I. Strakovsky,[11] M. Taiuti,[13] S. Taylor,[23] D. Tedeschi,[33] U. Thoma,[17] R. Thompson,[31] L. Todor,[3] T. Y. Tung,[6] C. Tur,[33] M. Ungaro,[1] M. F. Vineyard,[25] A. Vlassov,[14] K. Wang,[35] L. B. Weinstein,[21] H. Weller,[7] R. Welsh,[6] D. P. Weygand,[17] S. Whisnant,[33] M. Witkowski,[1] E. Wolin,[17] A. Yegneswaran,[17] J. Yun,[21] B. Zhang,[19] J. Zhao,[19] and Z. Zhou[19]

(CLAS Collaboration)

[1]*Rensselaer Polytechnic Institute, Troy, New York 12180, USA*
[2]*Arizona State University, Tempe, Arizona 85287, USA*
[3]*Carnegie Mellon University, Pittsburgh, Pennsylvania 15213, USA*
[4]*Catholic University of America, Washington D.C., 20064, USA*
[5]*Christopher Newport University, Newport News, Virginia 23606, USA*
[6]*College of William and Mary, Williamsburg, Virginia 23187, USA*
[7]*Duke University, Physics Building, TUNL, Durham, North Carolina 27706, USA*
[8]*Edinburgh University, Edinburgh EH9 3JZ, United Kingdom*
[9]*Florida International University, Miami, Florida 33199, USA*
[10]*Florida State University, Tallahassee, Florida 32306, USA*
[11]*George Washington University, Washington D.C., 20052, USA*
[12]*Istituto Nazionale di Fisica Nucleare, Laboratori Nazionali di Frascati, P.O. Box 13, 00044 Frascati, Italy*
[13]*Istituto Nazionale di Fisica Nucleare, Sezione di Genova e Dipartimento di Fisica dell'Universita, 16146 Genova, Italy*
[14]*Institute of Theoretical and Experimental Physics, 25 B. Cheremushkinskaya, Moscow, 117259, Russia*
[15]*Institut de Physique Nucleaire d'Orsay, IN2P3, Boîte Postale 1, 91406 Orsay, France*
[16]*James Madison University, Department of Physics, Harrisonburg, Virginia 22807, USA*
[17]*Thomas Jefferson National Accelerator Facility, 12000 Jefferson Avenue, Newport News, Virginia 23606, USA*
[18]*Kyungpook National University, Taegu 702-701, South Korea*
[19]*M.I.T.-Bates Linear Accelerator, Middleton, Massachusetts 01949, USA*
[20]*Norfolk State University, Norfolk, Virginia 23504, USA*
[21]*Old Dominion University, Norfolk, Virginia 23529, USA*
[22]*Ohio University, Athens, Ohio 45701, USA*
[23]*Rice University, Bonner Lab, Box 1892, Houston, Texas 77251, USA*
[24]*CEA Saclay, DAPNIA-SPhN, F91191 Gif-sur-Yvette Cedex, France*
[25]*Union College, Schenectady, New York 12308, USA*
[26]*University of California at Los Angeles, Los Angeles, California 90095, USA*
[27]*University of Connecticut, Storrs, Connecticut 06269, USA*
[28]*University of Massachusetts, Amherst, Massachusetts 01003, USA*

0556-2813/2003/68(3)/035202(14)/$20.00

[29]*University of Moscow, Moscow 119899 Russia*
[30]*University of New Hampshire, Durham, New Hampshire 03824, USA*
[31]*University of Pittsburgh, Pittsburgh, Pennsylvania 15260, USA*
[32]*University of Richmond, Richmond, Virginia 23173, USA*
[33]*University of South Carolina, Columbia, South Carolina 29208, USA*
[34]*University of Texas at El Paso, El Paso, Texas 79968, USA*
[35]*University of Virginia, Charlottesville, Virginia 22903, USA*
[36]*Virginia Polytechnic and State University, Blacksburg, Virginia 24061, USA*
[37]*Yerevan Physics Institute, 375036 Yerevan, Armenia*
(Received 17 March 2003; published 11 September 2003)

Measurements of the angular distributions of target and double-spin asymmetries for the $\Delta^+(1232)$ in the exclusive channel $\vec{p}(\vec{e},e'p)\pi^0$ obtained at the Jefferson Lab in the Q^2 range from 0.5 to 1.5 GeV$^2/c^2$ are presented. Results of the asymmetries are compared with the unitary isobar model [D. Drechsel *et al.*, Nucl. Phys. **A645**, 145 (1999)], dynamical models [T. Sato and T. S. Lee, Phys. Rev. C **54**, 2660 (1996); S. S. Kamalov *et al.*, Phys. Lett. B **27**, 522 (2001)], and the effective Lagrangian theory [R. M. Davidson *et al.*, Phys. Rev. D **43**, 71 (1991)]. Sensitivity to the different models was observed, particularly in relation to the description of background terms on which the target asymmetry depends significantly.

DOI: 10.1103/PhysRevC.68.0252XX PACS number(s): 13.60.Le, 13.88.+e, 14.20.Gk

I. INTRODUCTION

The $\Delta(1232)$ resonance has been one of the most studied objects in nuclear physics. As the lowest energy nucleon excitation it dominates the low energy cross sections for pion- and electromagnetic-induced reactions, and is almost completely separated in excitation energy from the many broad higher mass resonances. There is extensive theoretical literature attempting to characterize the electromagnetic excitation of the $\Delta(1232)$ resonance. Examples of some approaches are effective Lagrangian models [1–7], dispersion relations [8], partial-wave analysis [9], quark models [10,11], QCD sum-rule models [12], the generalized parton distribution approach [13,14], and perturbative QCD with QCD sum rules [15]. In recent years, there has been considerable experimental activity using polarized real photons at LEGS [16] and Mainz [17], unpolarized electrons at Bonn [18] and Jefferson Lab (JLab) [19,20], polarized electrons at Mainz [21] and JLab [22], and polarized electrons with recoil polarization at Mainz [23] and Bates [24], which have focused on constraining our understanding of the electromagnetic structure of the $\Delta(1232)$ resonance.

It has long been realized that the proper extraction of resonance information from experimental data requires an understanding of nonresonant contributions in the vicinity of the resonance pole. Some of the previously mentioned theoretical approaches have been developed to obtain a more realistic description of the full pion production amplitude and, in particular, the determination of the resonance contributions. It was found that certain polarization observables, e.g., single-spin asymmetries, where the polarization of only one particle is determined, are sensitive to interferences between resonant and nonresonant contributions, while double-polarization observables are more constrained by resonant contributions. Both contain information not contained in unpolarized cross sections alone.

The main aim of this paper is to present the results of a measurement of polarization observables in single π^0 electroproduction. It is expected that these results, together with other data will aid in reaching a better understanding of the most appropriate description of the complete pion production amplitude in the region of the $\Delta(1232)$ resonances.

Among the theoretical approaches that have appeared during the past several years with the aim of extracting resonance amplitudes from existing data are the aforementioned effective Lagrangian models [1] (MAID) and [4] [the Davidson-Mukhopadhyay (DM) model], in which the degrees of freedom are baryon and meson currents. These models include pion scattering effects by using the K-matrix method to unitarize the amplitude. The differences between the MAID and the DM models arise mainly from some rather significant differences in their starting effective Lagrangians. In particular, the MAID model uses a mixture of pseudoscalar and pseudovector for the πNN coupling, while the DM model uses the standard pseudovector coupling. The MAID model includes some higher resonances and hence has more freedom in fitting the data.

A major controversy which has developed is that the resonance amplitude calculated in the framework of the quark model [10] is significantly smaller than that extracted from effective Lagrangian models. Such a significant difference ($\sim$30%) for the presumably best understood resonance points to a very serious shortcoming for the quark model. However, it has been pointed out by the authors of Ref. [10] that the quark models—so far—are not able to take into account the coupling of the quarks to the pion cloud and, if this were rectified, one would expect better agreement with the amplitudes extracted from effective Lagrangian models.

With this in mind, an elaboration [2] of the effective Lagrangian model, the *dynamic model* [the Sato-Lee (SL) model], was developed in which the primary resonant and

*Corresponding author. Email address: biselli@jlab.org

nonresonant interactions involving the pion cloud are treated in a consistent coupled channel approach to all orders. This was followed by analogous dynamic formulations [7] (DMT). The SL model obtains the unitary amplitudes by solving dynamical πN scattering equations. Thus, the pion cloud effects on the extracted "dressed" $N-\Delta$ can be identified and an interpretation of the resulting "bare" parameters in terms of constituent quark model calculations has been established. The DMT model uses a chiral Lagrangian which includes the pion rescattering in a coupled channel t-matrix approach.

The net result yields a bare $\Delta(1232)$ resonance amplitude, stripped of its coupling with nonresonant channel dressed $\Delta(1232)$, which is smaller than that obtained in the more traditional effective Lagrangian formulations, and in better agreement with that obtained with the quark model. The coupling to all orders is also effected in the dispersion relation calculation [8], and again it is found that the bare $\Delta(1232)$ resonance agrees better with that of the quark model. The most important constraints for these models have been the high quality nonpolarized cross sections which have appeared in recent years [19,20].

The analysis of JLab unpolarized cross section data [19,20] using these various theoretical formalisms yield very different extracted nonleading amplitudes $\mathrm{Re}(E_{1+}/M_{1+})$ and $\mathrm{Re}(S_{1+}/M_{1+})$, depending on the model used. This is especially true with increasing momentum transfer, i.e., for Q^2 in the multi-GeV$^2/c^2$, where the relative contribution of the nonresonant amplitudes become more important relative to the resonant amplitudes. Thus, in order to obtain confident estimates of the resonant amplitudes one needs to determine which formulation best accounts for the overall body of the world's data.

In addition to the nonpolarized cross sections, these theoretical formulations can predict interference cross sections which can only be accessed by polarization variables. Of significance are the enhanced sensitivities to interferences between resonant and nonresonant amplitudes. Such interferences can offer strong constraints on models for extracting the interplay between resonant and nonresonant amplitudes. For example, in the case of the Mainz [21] single-electron asymmetry data $Q^2=0.2$ GeV$^2/c^2$, the predictions of some of the above theoretical formulations [2,7,1] differ significantly, and none give fully satisfactory agreements with the data. The authors speculated that the treatments of the nonresonant backgrounds may be the cause, though no quantitative comparisons between the different predictions and experiment were made. The JLab data [22] obtained at higher $Q^2=0.4$ and 0.65 GeV$^2/c^2$ were also compared with the results of the same theory and gave equally divergent results.

In the case of the Mainz [23] and Bates [24] recoil polarization experiments at $Q^2\sim 0.1$ GeV$^2/c^2$, comparisons were made with one of the models (MAID) to extract the $\Delta(1232)$ quadrupole amplitude $\mathrm{Re}(S_{1+}/M_{1+})$. However, since the different models are shown to yield different results for nonleading amplitudes when compared to other data, it would seem that one would need better confidence in the theoretical basis.

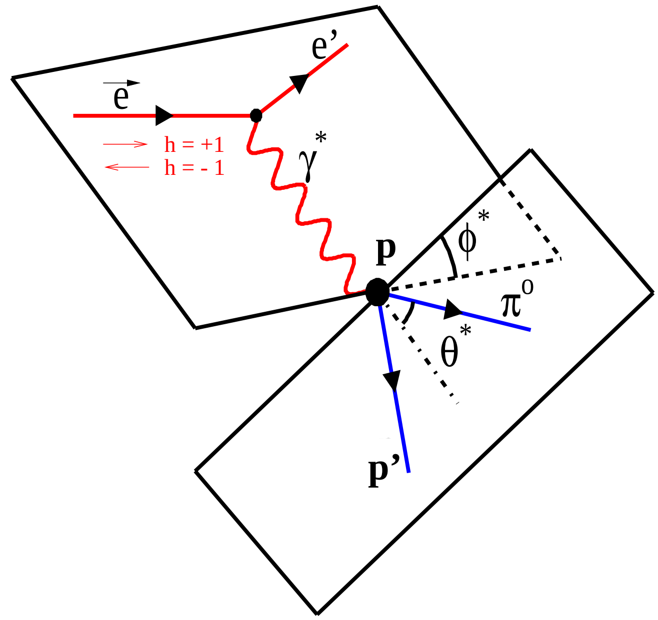

FIG. 1. (Color) Schematic diagram of π-nucleon electroproduction. $\vec{e}$ represents the incident polarized electron, e' is the outgoing electron, γ^* is the virtual photon, and p and p' are the nucleon in the initial and final state, respectively.

With this background in mind, the present report provides independent double-polarization data, which will be useful in testing the models, especially at previously unexplored higher Q^2 (0.5–1.5 GeV$^2/c^2$), where new physics may open up and background effects become relatively more important. The reaction studied in the presently reported experiment is $\vec{e}+\vec{p}\rightarrow e'+p+\pi^0$, where the scattered electron and emitted proton were observed in coincidence, and the π^0 was identified by the missing mass technique. Although the feasibility of exclusive coincidence experiments involving target and beam double polarization was demonstrated in the reaction $\vec{e}+\vec{p}\rightarrow e'+n+\pi^+$ in Ref. [25], this is the first time such experiments are carried out in which the Q^2 behavior of the target and double-spin asymmetries for a specific resonance are explored in the GeV range of momentum transfer. We expect these unique polarization observables to give significant constraints for improving theories of the $\Delta(1232)$ electroproduction process.

In addition, quantitative comparisons are made to the predictions of the four theoretical approaches: MAID [1], SL [2], DMT [3], and DM [4].

II. FORMALISM

In this experiment, single mesons are produced by a polarized electron beam incident on a polarized proton target polarized parallel or antiparallel to the electron beam direction, as schematically shown in Fig. 1. The incident polarized electron is given by the four-vector $p_e=(\vec{p}_e,E_i)$, the outgoing electron is emitted with angles ϕ_e,θ_e and four-vector $p_e'=(\vec{p}_e\,',E_f)$, the virtual photon is characterized by q

$=(\vec{q},\omega)$ where $\vec{q}=\vec{p}_e-\vec{p}_e^{\,\prime}$ and $\omega=E_i-E_f$, and the nucleon initial and final states are given by $p_p=(0,M)$ and $p_p'=(\vec{p}_p,E_p)$, respectively. In terms of these variables, the cross section can be written as

$$\frac{d\sigma}{dE_f d\Omega_e d\Omega^*}=\Gamma\frac{d\sigma}{d\Omega^*}, \tag{1}$$

where $d\Omega_e=\sin\theta_e d\theta_e d\phi_e$ is the electron solid angle, $d\Omega^*=\sin\theta^* d\theta^* d\phi^*$ is the solid angle of the meson in the center of mass,

$$\Gamma=\frac{\alpha}{2\pi^2}\frac{E_f}{E_i}\frac{k_\gamma^{lab}}{Q^2}\frac{1}{1-\epsilon} \tag{2}$$

is the virtual photon flux,

$$\epsilon=\left(1+2\frac{|\vec{q}|^2}{Q^2}\tan^2\frac{\theta_e}{2}\right)^{-1} \tag{3}$$

represents the degree of polarization of the virtual photon,

$$k_\gamma^{lab}=\frac{W^2-M^2}{2M} \tag{4}$$

denotes the ‘‘photon equivalent energy’’ necessary for a real photon to excite a hadronic system with center-of-mass (c.m.) energy $W=|p_e+p_p-p_e'|$, $Q^2=-q^2=-(\omega^2-\vec{q}^{\,2})$ is the momentum transfer, and α is the fine structure constant. The differential cross section for pion production by a virtual photon $d\sigma/d\Omega^*$ can be written as a sum of four terms as follows:

$$\frac{d\sigma}{d\Omega^*}=\frac{|\vec{k}|}{k_\gamma^{c.m.}}\left\{\frac{d\sigma_0}{d\Omega^*}+h\frac{d\sigma_e}{d\Omega^*}+P\frac{d\sigma_t}{d\Omega^*}-hP\frac{d\sigma_{et}}{d\Omega^*}\right\}, \tag{5}$$

where $\vec{k}$ is the momentum of the pion, h is the electron helicity, and P is the target proton polarization. The first term $d\sigma_0/d\Omega^*$ represents the unpolarized cross section, while the remaining terms $d\sigma_e/d\Omega^*$, $d\sigma_t/d\Omega^*$, and $d\sigma_{et}/d\Omega^*$ arise when beam, target, or both beam and target are polarized, respectively. Here,

$$k_\gamma^{\text{c.m.}}=\frac{M}{W}k_\gamma^{lab} \tag{6}$$

is the real photon equivalent energy in the c.m. frame. These cross sections can be written in terms of response functions R using the formalism of Ref. [26] as

$$\frac{d\sigma_0}{d\Omega^*}=R_T^0+\epsilon_L R_L^0+\sqrt{2\epsilon_L(1+\epsilon)}R_{TL}^0\cos\phi^*+\epsilon R_{TT}^0\cos 2\phi^*, \tag{7}$$

$$\frac{d\sigma_e}{d\Omega^*}=\sqrt{2\epsilon_L(1-\epsilon)}R_{TL'}^0\sin\phi^*,$$

$$\begin{aligned}\frac{d\sigma_t}{d\Omega^*}=&\sin\theta_\gamma\cos\phi^*[\sqrt{2\epsilon_L(1+\epsilon)}R_{TL}^x\sin\phi^*\\&+\epsilon R_{TT}^x\sin 2\phi^*]+\sin\theta_\gamma\sin\phi^*[R_{TL}^y+\epsilon_L R_L^y\\&+\sqrt{2\epsilon_L(1+\epsilon)}R_{TL}^y\cos\phi^*+\epsilon R_{TT}^y\cos 2\phi^*]\\&+\cos\theta_\gamma[\sqrt{2\epsilon_L(1+\epsilon)}R_{TL}^z\sin\phi^*+\epsilon R_{TT}^z\sin 2\phi^*],\end{aligned}$$

$$\begin{aligned}\frac{d\sigma_{et}}{d\Omega^*}=&-\sin\theta_\gamma[\sqrt{2\epsilon_L(1-\epsilon)}R_{TL'}^x\cos\phi^{*2}\\&+\sqrt{1-\epsilon^2}R_{TT'}^x\cos\phi^*]\\&+\sin\theta_\gamma\sqrt{2\epsilon_L(1-\epsilon)}R_{TL'}^y\sin\phi^{*2}\\&-\cos\theta_\gamma[\sqrt{2\epsilon_L(1-\epsilon)}R_{TL'}^z\cos\phi^*+\sqrt{1-\epsilon^2}R_{TT'}^z],\end{aligned}$$

where

$$\epsilon_L=\frac{Q^2}{\omega^2}\epsilon \tag{8}$$

is the frame-dependent longitudinal polarization the virtual photon. The θ_γ is the angle between the directions of the target polarization and virtual photon.

The asymmetries are then defined as follows:

$$A_e=\frac{\sigma_e}{\sigma_0},$$

$$A_t=\frac{\sigma_t}{\sigma_0},$$

$$A_{et}=\frac{\sigma_{et}}{\sigma_0}, \tag{9}$$

where $\sigma_0\equiv d\sigma_0/d\Omega^*$, $\sigma_e\equiv d\sigma_e/d\Omega^*$, $\sigma_t\equiv d\sigma_t/d\Omega^*$, and $\sigma_{et}\equiv d\sigma_{et}/d\Omega^*$.

III. EXPERIMENTAL SETUP

The experiment was carried out from September to December 1998 using the CEBAF Large Acceptance Spectrometer (CLAS) at JLab, using a polarized electron beam of energy $E=2.565$ GeV at an average beam current of about 2 nA. Pairs of complementary helicity states were created pseudorandomly by a pockel cell producing circularly polarized laser light, which is used to generate polarized electrons from a strained GaAs photocathode [27]. Each pair of complementary helicity states had a duration of 2 sec. Helicity-correlated systematic uncertainties are reduced by selecting the first helicity of the pair pseudorandomly. The average polarization of the beam for the entire dataset, measured with a Møller polarimeter, was $P_e=0.71\pm0.01$. The beam was rastered in a spiral pattern of 1–1.2 cm diameter over the surface of the target to avoid destroying the target polarization.

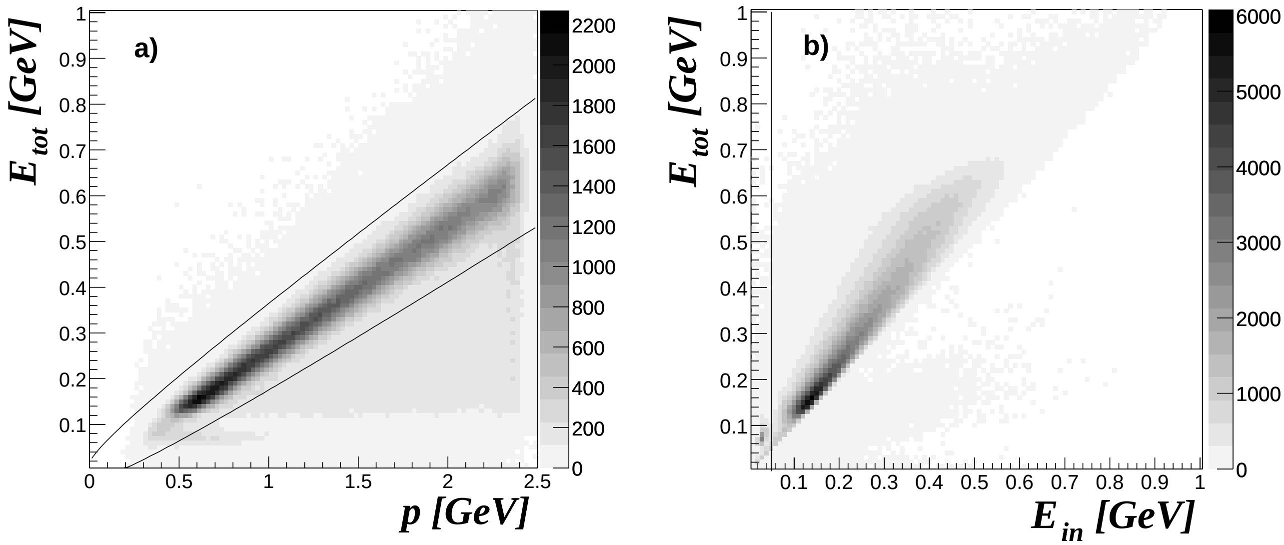

FIG. 2. Electron identification. (a) E_{tot} vs p. The two lines indicate the cut applied to remove the events that deviate by more than three σ from the expected behavior. (b) E_{tot} vs E_{in}. The line indicates the cut applied to remove the events that have E_{in} much smaller than E_{tot}, which correspond to misidentified pions.

The electrons impinged on a solid ammonia (NH_3) target of thickness 530 mg/cm^2, in which the free protons were longitudinally polarized. The target polarization was changed every 2–3 weeks. *Dynamic nuclear polarization* [28,29] was used to polarize this target using a 5 T uniform holding-field generated by a superconducting Helmholtz-like coil placed axially around the target. This coil limited the available scattering angles to less than 45° and between 70° and 110°. A more complete description of the target and polarization technique may be found in Ref. [30]. Typically, the polarizations achieved for positive and negative polarizations were about 39% and 55%, respectively. The effective instantaneous luminosity for the polarized hydrogen was about 6.6×10^{32} cm^{-2} s^{-1}.

Scattered electrons and recoiled protons were detected in the CLAS, which is described in detail in Ref. [31]. An event was triggered when a coincidence between the threshold Cherenkov counter (CC) and the electromagnetic calorimeter (EC) was detected. A typical Cherenkov signal consisted of 6–12 photoelectrons (PE), with an average of about 10. The trigger threshold was set at 0.5 PE. Electron candidates were identified by a combination of time-of-flight (TOF) scintillators, CC, and EC. The TOF scintillators completely surround the drift chambers, whereas the EC and the CC subtend angles less than 45° with respect to the beam line. The momenta of the detected particles were determined by fitting their measured trajectories in the toroidal field, which curves the tracks in the θ direction but leaves them nearly unaffected in the ϕ direction. The trajectories are determined by three sets of drift chambers (DC), the inner most having ten layers and the other two having each 12 layers of drift cells.

IV. DATA REDUCTION AND ANALYSIS

A. Electron identification

Electron identification was improved off-line in order to remove pions and other sources of contamination. The EC signal was used to remove events in which tracks triggered the CC but did not shower in the EC, such as pions which generate secondary electrons. The energy released by electrons traversing the EC is proportional to the momentum p as shown in Fig. 2(a). The width of the band is due to the EC resolution and the lines indicate the cut applied to remove background. The EC signal is also measured separately for the inner part (15 layers of scintillators) and outer part (24 layers). This allows one to distinguish between an electron, which showers mostly in the inner part, and minimum ionizing particles, such as π's, which lose most of their energy

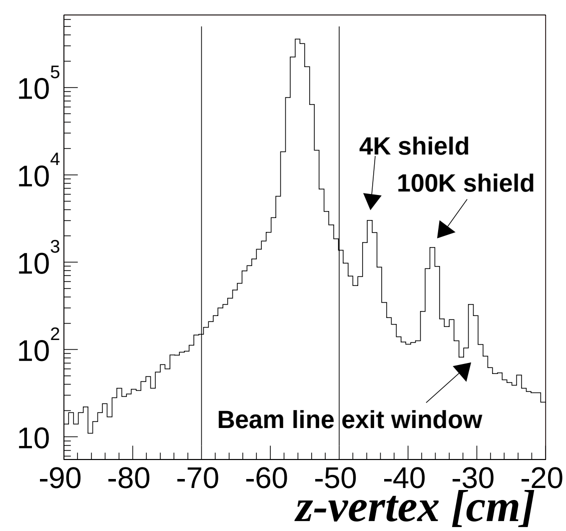

FIG. 3. The number of events as a function of the vertex z position of the electron where z is along the beamline. The lines, which indicate the applied cut, show that the peaks resulting from the scattering off the target temperature shields and the beam line exit window are completely removed. (Note the logarithm vertical scale). The cut does not remove the exit and entrance windows from the target cell.

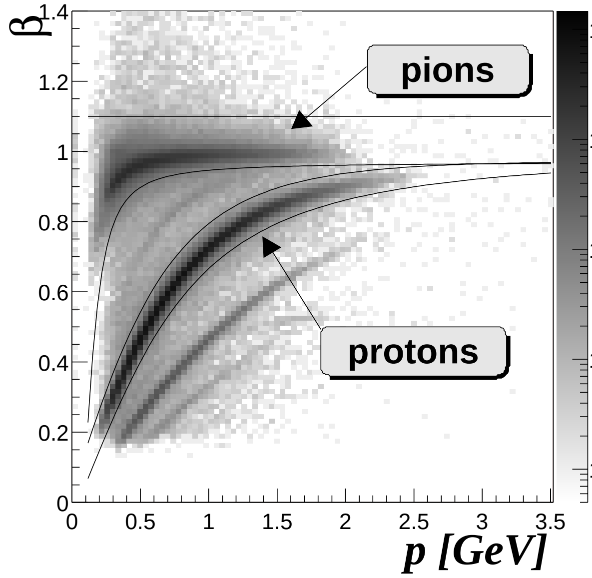

FIG. 4. β vs p for all positive charge particles. The lines show how pions and protons are easily distinguishable.

in the outer part. This behavior is evident in Fig. 2(b) where the high intensity region with $E_{in} \sim E_{tot}$ corresponds to electrons, while the small peak at low E_{in} corresponds to misidentified pions. The vertical line indicates the cut applied to remove misidentified pions.

The reconstructed vertex position was used to remove events originating from the target temperature shields and the beam line exit window. Figure 3 shows the cut applied to selected events from inside the target.

B. Proton identification

Protons were identified by determining their momentum and path length using the DC, and their $\beta = v/c$ using the TOF. Figure 4 shows the cut applied to select protons, which appear well separated from the pions for momenta less than 2 GeV/c.

C. π^0 channel identification

In order to select the $\Delta(1232)$ resonance in the decay channel $\Delta^+ \to \pi^0 p$, cuts on the invariant mass W and the square of the missing mass $M_X^2 = |p_e + p_p - p_e' - p_p'|^2$ were performed. The $^{15}NH_3$ target intrinsically has a large background due to scattering from bound nucleons in ^{15}N. Many of these events were removed through kinematic cuts. An initial two-dimensional cut was applied to select the $\Delta(1232)$ region and to remove the elastic and quasielastic events as shown in Fig. 5(a). The underlying quasi-Δ events from ^{15}N, not kinematically separable, were removed by a subtraction process by comparing to data taken with a ^{12}C target. Figure 5(b) shows the missing mass spectrum obtained with $^{15}NH_3$ and ^{12}C targets after the two-dimensional cut and the resulting subtraction. The remaining pion peak due to H is narrower than the $^{15}NH_3$ peak. A second and much tighter cut on M_X^2 alone was therefore performed to optimize the selection of pions from reactions on free hydrogen in $^{15}NH_3$. The two vertical lines in Fig. 5(b) show the applied cut.

D. Elastic radiative tail

The elastic radiative tail was suppressed by the presence of the target magnetic coils that block polar angles between

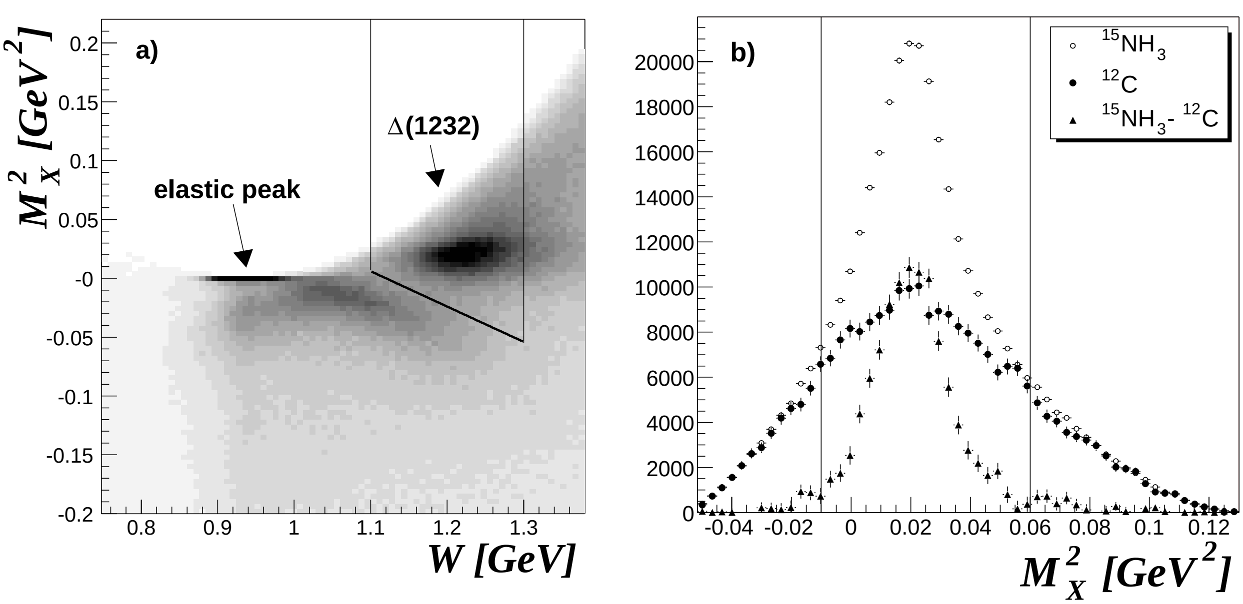

FIG. 5. Identification of $p\pi^0$ events. (a) M_X^2 vs W. The lines show the two-dimensional cut applied in order to remove the elastic events and quasielastic shoulder. (b) The plot shows the resulting M_X^2 spectrum after the two-dimensional cut (open circles), the ^{12}C data normalized to the $^{15}NH_3$ target data (full circles), and the difference of the two (triangles). The two lines show the final cut in M_X^2 to select pions scattering off hydrogen.

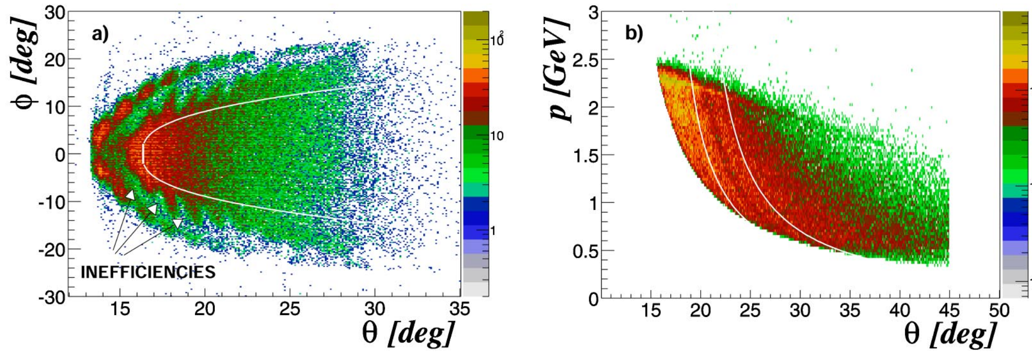

FIG. 6. (Color) (a) ϕ vs θ for electrons in the first CLAS sector for a momentum (p) bin from 1.9 to 2.1 GeV/c. The line indicates the cut applied to remove the external fringes and the depletion due to CC inefficiencies. (b) p vs θ for electrons in the third CLAS sector after applying the cut shown in (a). The region inside the two lines corresponds to an inefficient scintillator.

45° and 70°. The remaining elastic radiative events were removed by means of a cut on the reconstructed electron scattering angle (θ) [32]. This cut removed 15% of the original dataset.

E. Fiducial cuts and acceptance corrections

The efficiency can vary by more than an order of magnitude near the boundaries of the six azimuthal sectors of CLAS, therefore only events in the region where the acceptance is uniform were included. Limiting electrons to this fiducial region, gives an elastic scattering cross section that is consistent with the world's data to within a few percent. Although the objective of the present analysis is to extract asymmetries, a good understanding of the acceptance is necessary. Calculating the asymmetries involves integrations over ranges in Q^2, ϕ^*, θ^*, and W, and since the acceptance is a function of these variables, it does not cancel out when ratios of the integrated quantities are taken. Fiducial cuts define a region in θ and ϕ depending on the momentum for both the electron and the proton. The area inside the line in Fig. 6(a) is an example of the region selected by the fiducial cuts for electrons detected in the first CLAS sector and with momenta between 1.9 GeV/c and 2.1 GeV/c. The cuts not only remove data close to the sector boundaries, but further remove events from regions where scintillators are inefficient or which have other tracking inefficiencies. Figure 6(b) displays the effect of a cut to remove an inefficient scintillator in the third CLAS sector. The total amount of data removed by the fiducial cuts for events with one electron and one proton and $W<1.4$ GeV/c^2 is of the order of 60%. Data were ϕ acceptance corrected event by event using an analytical calculation based on the assumption that acceptance within the fiducial region is 100%. Figure 7 shows the acceptance as a function of ϕ^* and θ^* calculated for two intervals in Q^2 within a W range of 1.1–1.3 GeV/c^2.

F. Experimental definition of the asymmetries

The experimentally measured number of counts, N_{ij}, are grouped according to different combinations of beam (i) and target (j) polarizations. Under the assumption of constant efficiency, these may be written in terms of the cross sections in Eqs. (7) as

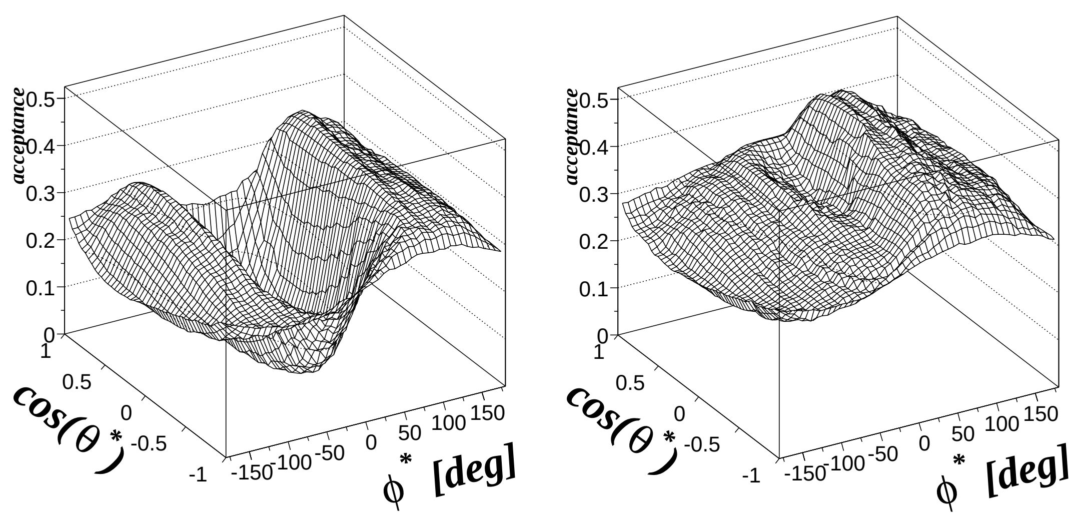

FIG. 7. Acceptance calculation for two intervals in Q^2 for 1.1 GeV/$c^2<W<1.3$ GeV/c^2. The lower interval has a region around $\phi^*=0°$ where the acceptance is zero.

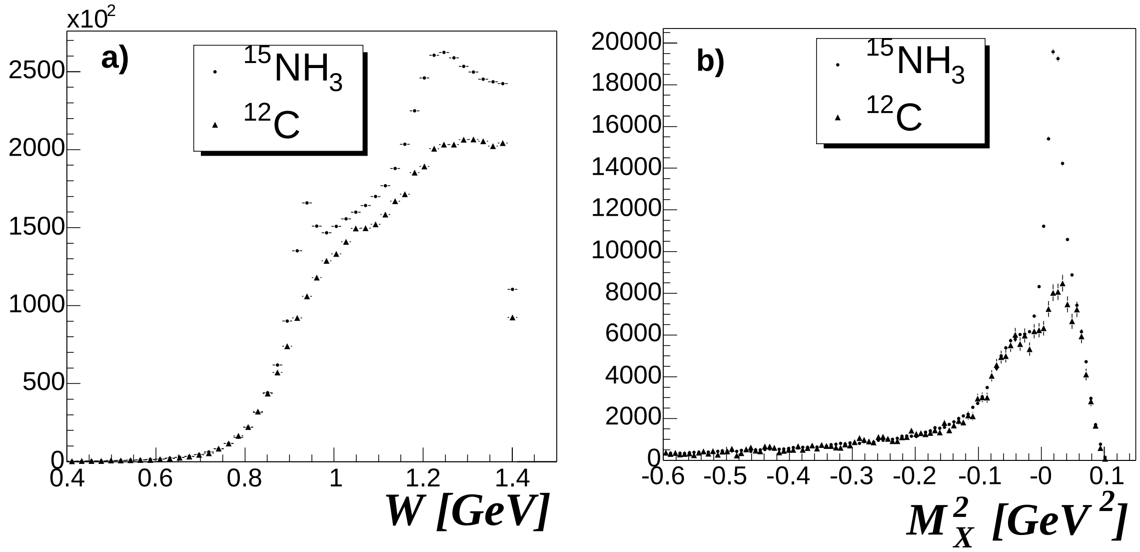

FIG. 8. (a) Exclusive W spectra for $^{15}NH_3$ (circles) and ^{12}C (triangles). The spectra are normalized to each other using the integrals of the W tails in the range 0.6 GeV/c^2 to 0.85 GeV/c^2. (b) Overlay of M_X^2 spectra for $^{15}NH_3$ (circles) and ^{12}C (triangles). The ^{12}C was normalized using the constant found from the W tail integrals.

$$\begin{aligned}
N_{\uparrow\uparrow} &\propto (\sigma_0+\sigma_0^N+P_e\sigma_e+P_e\sigma_e^N+P_t^a\sigma_t-P_eP_t^a\sigma_{et}),\\
N_{\downarrow\uparrow} &\propto (\sigma_0+\sigma_0^N-P_e\sigma_e-P_e\sigma_e^N+P_t^a\sigma_t+P_eP_t^a\sigma_{et}),\\
N_{\uparrow\downarrow} &\propto (\sigma_0+\sigma_0^N+P_e\sigma_e+P_e\sigma_e^N-P_t^b\sigma_t+P_eP_t^b\sigma_{et}),\\
N_{\downarrow\downarrow} &\propto (\sigma_0+\sigma_0^N-P_e\sigma_e-P_e\sigma_e^N-P_t^b\sigma_t-P_eP_t^b\sigma_{et}),
\end{aligned} \tag{10}$$

where σ_0^N and σ_e^N are the contributions from the scattering from ^{15}N and the liquid helium coolant, and P^a and P^b are the magnitudes of positive and negative target polarizations, respectively. The left-hand sides of these equations (N_{ij}) have been normalized to the same total beam charge. The asymmetries may be written in terms of these quantities as

$$\begin{aligned}
A_t &= \frac{\sigma_t}{\sigma_0} = \frac{1}{P_t^b}\frac{(N_{\uparrow\uparrow}+N_{\downarrow\uparrow})-(N_{\uparrow\downarrow}+N_{\downarrow\downarrow})}{(N_{\uparrow\uparrow}+N_{\downarrow\uparrow})+\alpha(N_{\uparrow\downarrow}+N_{\downarrow\downarrow})-\beta\sigma_0^N},\\
A_{et} &= \frac{\sigma_{et}}{\sigma_0} = \frac{1}{P_eP_t^b}\frac{-(N_{\uparrow\uparrow}-N_{\downarrow\uparrow})+(N_{\uparrow\downarrow}-N_{\downarrow\downarrow})}{(N_{\uparrow\uparrow}+N_{\downarrow\uparrow})+\alpha(N_{\uparrow\downarrow}+N_{\downarrow\downarrow})-\beta\sigma_0^N},
\end{aligned} \tag{11}$$

where

$$\alpha = \frac{P_t^a}{P_t^b} \tag{12}$$

and

$$\beta = 2(1+\alpha). \tag{13}$$

Extraction of the nuclear background cross section σ_0^N and constant α are discussed in the next two sections.

G. Background subtraction

The data have a large background σ_0^N due to scattering from ^{15}N and the helium cooling bath. Data taken with ^{12}C and ^{4}He targets were used to remove this contribution. While the ^{12}C and ^{15}N targets had similar radiation lengths, they displaced different amounts of helium. A two-step procedure to handle this problem was employed. The first step was to determine how to add ^{12}C and empty target data properly in order to have the same ratio of heavier nuclei and helium as in the $^{15}NH_3$ data. Using a calculation based on the target thicknesses, densities, and window contributions, the background spectrum was calculated as $N^{BG}=N^C$

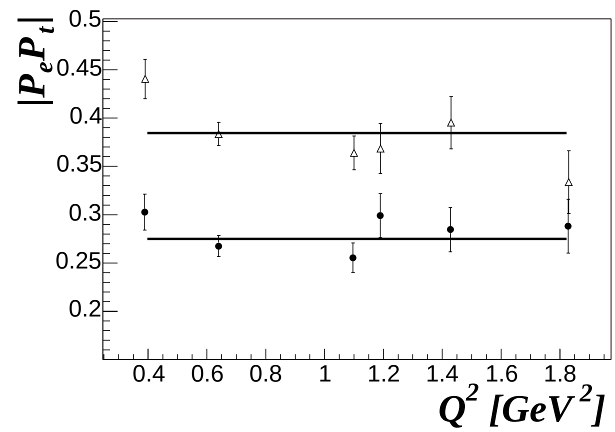

FIG. 9. The product $|P_eP_t|$ as a function of Q^2 for positive (filled circles) and negative (open triangles) target polarization runs. The six values for each polarization were fitted with a constant in order to obtain the average values $P_eP_t^a=0.275\pm0.007$ and $P_eP_t^b=-0.385\pm0.008$. The values for the χ^2 per degree of freedom of the fits were 5.884/5 and 11.87/5, respectively (note suppressed zero).

$-(0.331 \pm 0.008)N^E$, where N^C and N^E are the total number of ^{12}C and empty target data, respectively, normalized to the same charge.

The second step in the background subtraction was to determine a cross-normalization constant C_Δ, which allows N^{BG} to be equivalent to the rates from ^{15}N, accounting for the different ratios of protons to neutrons between the two backgrounds. A constant for the elastic region, C_{el}, was found as a ratio of the integrals of the W tails of $^{15}NH_3$ and the background data from $W = 0.6$–0.85 GeV/c^2, where only events from scattering by bound nucleons are present. Figure 8(a) shows the overlay of the W spectra of $^{15}NH_3$ and ^{12}C after normalization by C_{el}. A correction for higher W was then applied to C_{el} to account for rates by the scattering off neutrons. $C_\Delta = \frac{6}{7}\frac{22}{18}C_{el}$ was obtained for the $\Delta(1232)$ region, where $\frac{6}{7}$ is the ratio of protons in ^{12}C and ^{15}N and $\frac{22}{18}$ is based on a Clebsch-Gordan coefficient analysis [32]. Figure 8(b) shows the overlay of M_x^2 for $^{15}NH_3$ and background data after normalization using C_Δ. The tails where $M_x^2 < 0$ match, as expected, since they result only from the quasielastic scattering off the bound nucleons. The technique was later verified using a ^{15}N target.

H. Target polarization measurement

The target polarization was extracted by comparing the well known elastic scattering asymmetry [33]

$$A_{theo} = -\frac{\cos\theta_\gamma\sqrt{1-\epsilon^2} + \left(\dfrac{Q^2}{4M^2}\right)^{-1/2}\sqrt{2\epsilon(1-\epsilon)}\sin\theta_\gamma\cos\phi_\gamma\dfrac{G_E}{G_M}}{\epsilon\left(\dfrac{Q^2}{4M^2}\right)^{-1}\left(\dfrac{G_E}{G_M}\right)^2 + 1} \tag{14}$$

with the measured asymmetry

$$A_{meas} = \frac{N_{\uparrow\uparrow} - N_{\downarrow\uparrow}}{N_{\uparrow\uparrow} + N_{\downarrow\uparrow}} = \frac{P_e P_t \sigma_{et}}{\sigma_0} \equiv P_e P_t A_{theo}. \tag{15}$$

The ratio G_E/G_M has been measured in many experiments and it is known within a 3% accuracy in the Q^2 region of interest [34]. The product of beam and target polarization ($P_e P_t$) was independently estimated using six Q^2 bins and then the average value was calculated. Figure 9 shows the results for the positive ($P_e P_t^a$) and negative target polarization data ($P_e P_t^b$). These measurements allow one to extract target polarizations P_t^a, P_t^b by simply taking the ratio of these products and the measured beam polarization P_e (see Sec. III).

I. Systematic uncertainties

Several sources of possible systematic effects were identified in the analysis procedure. To estimate the size of these uncertainties, asymmetries were recalculated changing individual parameters in the analysis and comparing with the original result. Table I summarizes the systematic uncertainties for A_{et} in the bin 0.9 GeV^2/$c^2 < Q^2 < 1.5$ GeV^2/c^2. Similar values were found for the other asymmetries and Q^2 bins. The overall systematic uncertainty is of the order of 5 %, which is much smaller than the statistical uncertainty for the measured asymmetries.

TABLE I. Summary of the systematic uncertainties for the asymmetry A_{et} for 0.9 GeV^2/$c^2 < Q^2 < 1.5$ GeV^2/c^2.

Systematic uncertainty source	Systematic uncertainty (%)
Carbon normalization	4.2
$P_e P_t$	2.3
P_e	1.3
^{4}He background contribution	3.3

J. Radiative corrections

Radiative corrections were estimated using a generalization of the Mo-Tsai formulation [35]. In particular, the corrections were obtained by comparing Monte Carlo generated radiative and nonradiative events. The regions with zero acceptance existing in the data were incorporated in the Monte

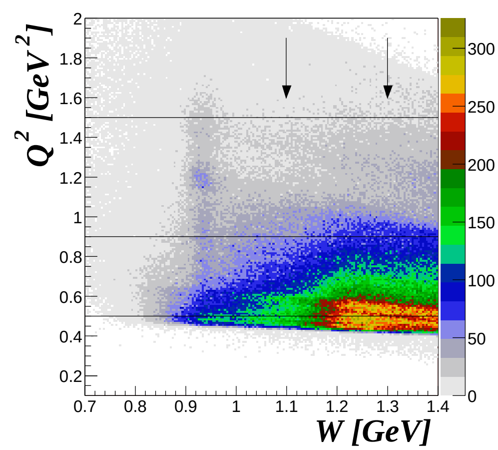

FIG. 10. (Color) Q^2 vs W. In the $\Delta(1232)$ region, the accessible range in Q^2 is from 0.4 GeV^2/c^2 to 1.5 GeV^2/c^2. The horizontal lines delineate the two intervals of Q^2 in which the data were divided.

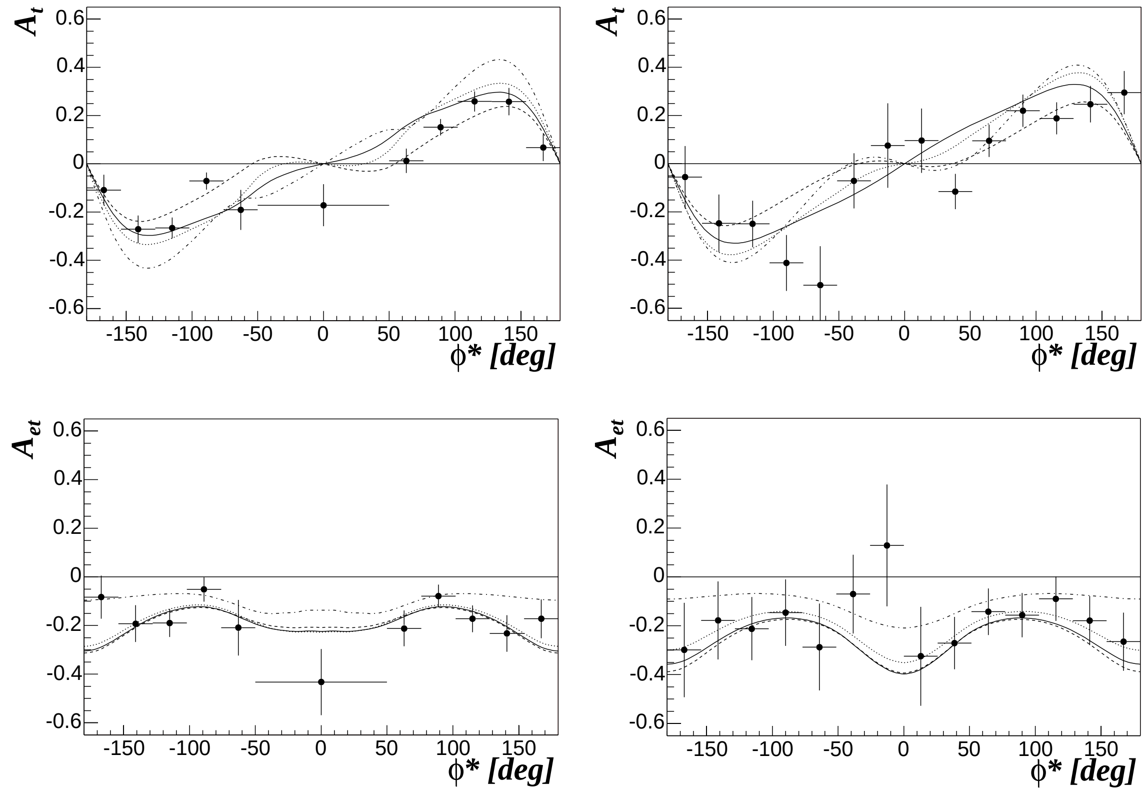

FIG. 11. Asymmetries A_t and A_{et} as a function of the center-of-mass angle of the pion ϕ^* integrated over cos θ^* for 0.5 GeV$^2/c^2$ $<Q^2<0.9$ GeV$^2/c^2$ (left) and 0.9 GeV$^2/c^2<Q^2<1.5$ GeV$^2/c^2$ (right). The curves represent the predictions from the MAID2000 model (solid), the Davidson-Mukhopadhyay model (dash-dotted), the Sato-Lee model (dashed), and the DMT model (dotted).

Carlo simulation in order to improve the model representation of the data. The difference between asymmetries calculated with radiative and nonradiative events revealed that radiative corrections influence the data by at most a few percent.

V. RESULTS

Data for a beam energy of 2.565 GeV, within the $\Delta(1232)$ region (1.1 GeV/$c^2<W<1.3$ GeV/c^2), span a range in momentum transfer Q^2 from 0.4 GeV$^2/c^2$ to 1.5 GeV$^2/c^2$, as can be seen in Fig. 10. The data were divided in two Q^2 bins, 0.5 GeV$^2/c^2<Q^2<0.9$ GeV$^2/c^2$ and 0.9 GeV$^2/c^2<Q^2<1.5$ GeV$^2/c^2$, and the asymmetries A_t and A_{et} were extracted according to the definitions in Eqs. (11) as a function of the angle of the pion in the center of mass ϕ^*, integrated over cos θ^*, and conversely as a function of cos θ^*, integrated over ϕ^*. The Q^2 dependences integrated over ϕ^* and cos θ^* were extracted as well. The results are shown in Figs. 11–13 and listed in Tables II–VI. The beam asymmetry was not extracted because it could not be separated from the background stemming from $\Delta(1232)\to\pi^- p$ that is produced by the scattering of neutrons in ^{15}N.

According to Eq. (7) the asymmetries depend on $\sin\phi^*$, $\cos\phi^*$, $\sin 2\phi^*$, and $\cos 2\phi^*$, giving a well defined functional dependence in ϕ^* that is model independent, and the data were found to agree with this expectation. The target asymmetry was found to be an odd function, and a fit to the function $(A\cos\phi^*\sin\phi^*+B\sin\phi^*+C\sin^3\phi^*)/D+E\cos\phi^*+F\cos 2\phi^*$ gave χ^2 per number of degree of freedom (ndf) values of 7.9/9 and 15.4/9 for the low and high Q^2 bin respectively. The double spin asymmetry was fitted with the even function $(A+B\cos\phi^*+C\cos^2\phi^*)/D+E\cos\phi^*+F\cos 2\phi^*$ and the values $\chi^2/\mathrm{ndf}=4.4/9$ for 0.5 GeV$^2/c^2$ $<Q^2<0.9$ GeV$^2/c^2$ and 4.8/7 for 0.9 GeV$^2/c^2<Q^2$ <1.5 GeV$^2/c^2$ were found.

A. Comparison with models

As noted in the Introduction, comparisons of the present results with four theoretical approaches were carried out. These include MAID2000 [1] (MAID), an effective Lagrangian model [4] (DM), and the dynamical models of SL [2,5] and DMT [3].

B. χ^2 comparison

All the models predict the correct sign and the correct order of magnitude, but do not yield equally good overall fits to the data. A simultaneous χ^2 comparison of all angular distributions, as well as the Q^2 distributions were performed to establish quantitatively which model gives the best description of the data. A χ^2 comparison for subsets of the experimental distributions was performed as well to understand the model sensitivity to the different asymmetries. In

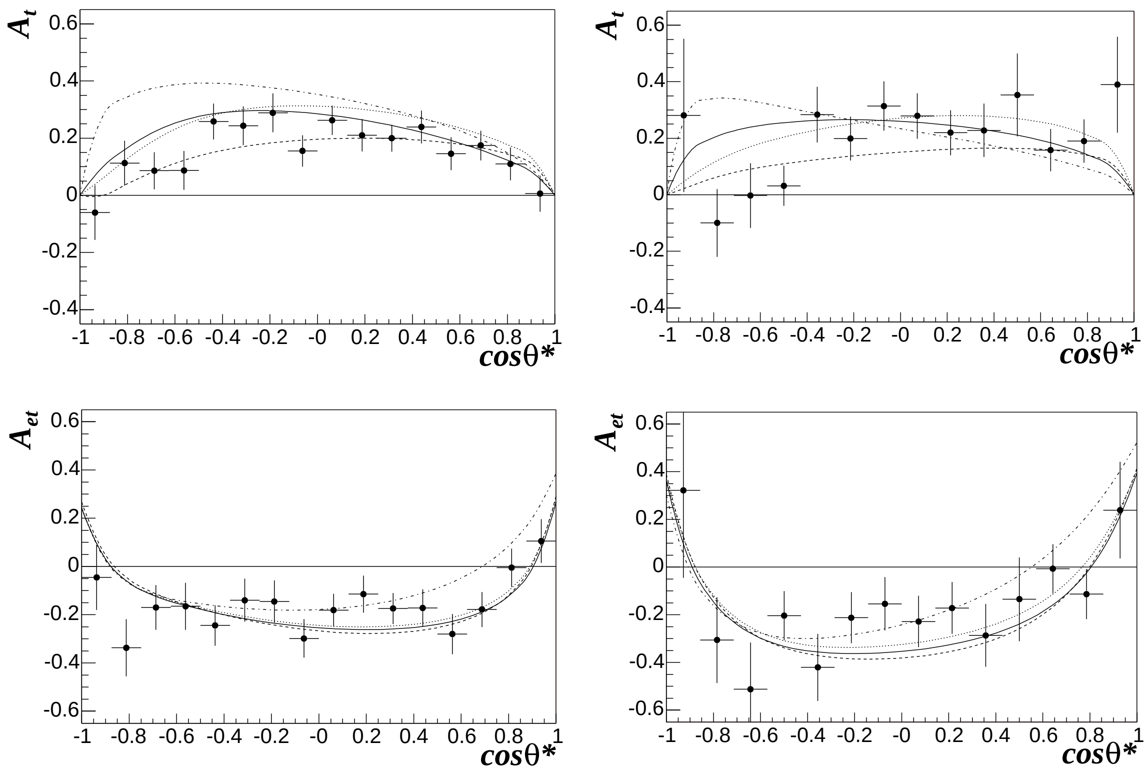

FIG. 12. Asymmetries A_t and A_{et} as a function of the center-of-mass angle of the pion $\cos\theta^*$ integrated over $0° < \phi^* < 180°$ and $-180° < \phi^* < 180°$, respectively, for $0.5\ \mathrm{GeV}^2/c^2 < Q^2 < 0.9\ \mathrm{GeV}^2/c^2$ (left) and $0.9\ \mathrm{GeV}^2/c^2 < Q^2 < 1.5\ \mathrm{GeV}^2/c^2$ (right). The curves represent the predictions from the MAID2000 model (solid), the Davidson-Mukhopadhyay model (dash-dotted), the Sato-Lee model (dashed), and the DMT model (dotted). Note that the complete data set contributes to the determination of A_t by making use of the symmetry of σ_t with respect to ϕ^*. This was achieved by integrating the terms for σ_t in Eqs. (11) for positive and negative ϕ^* separately and then adding the two results with opposite sign. Also, note that the results for the lower Q^2 bin are affected by the zero acceptance region (see Fig. 7).

order for a χ^2 comparison to be made, the model prediction was disregarded where the acceptance was zero.

The χ^2 was defined as

$$\chi^2 = \sum_i \frac{(x_i^{\mathrm{data}} - x_i^{\mathrm{model}})^2}{(\sigma_i^{\mathrm{data}})^2}, \tag{16}$$

where x_i^{data} is the value of each experimental point for all the asymmetries and x_i^{model} is the corresponding value of the theoretical prediction. Since the model is given without errors, only the experimental uncertainties σ_i^{data} were used in the denominator.

All the curves shown in this section display the exact point-by-point model prediction. In order to compare the

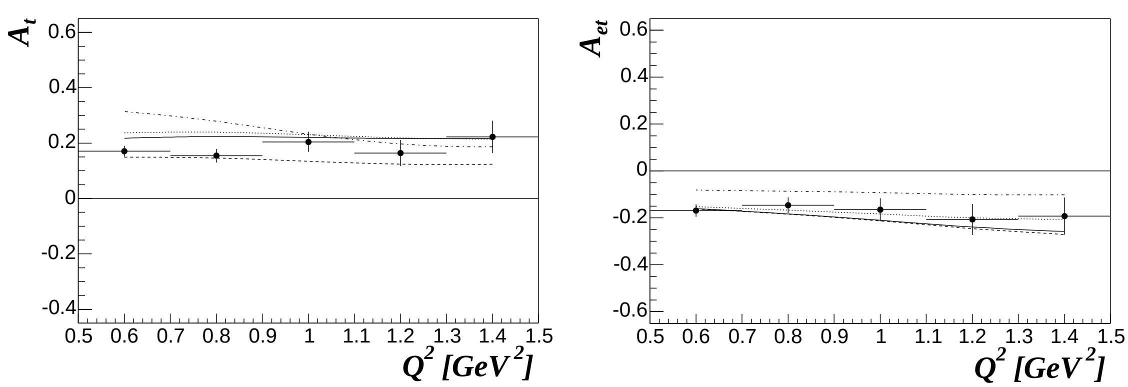

FIG. 13. Asymmetries A_t and A_{et} as a function of the momentum transfer Q^2 integrated over $\cos\theta^*$ and $0° < \phi^* < 180°$ and $-180° < \phi^* < 180°$, respectively. The curves represent the predictions from the MAID2000 model (solid black), the Davidson-Mukhopadhyay model (dash-dotted), the Sato-Lee model (dashed), and the DMT model (dotted).

TABLE II. Asymmetries A_t and A_{et} as a function of center-of-mass angle of the pion ϕ^* integrated over $\cos\theta^*$ at low Q^2. The uncertainties listed are statistical and systematic, respectively.

	$0.5\ \mathrm{GeV}^2/c^2 < Q^2 < 0.9\ \mathrm{GeV}^2/c^2$	
ϕ^* (deg)	A_t	A_{et}
−167.0	−0.108±0.063±0.008	−0.083±0.088±0.006
−141.0	−0.271±0.058±0.018	−0.192±0.076±0.014
−115.0	−0.266±0.044±0.016	−0.189±0.058±0.012
−89.0	−0.071±0.036±0.006	−0.052±0.050±0.003
−63.0	−0.191±0.083±0.012	−0.209±0.115±0.017
0.0	−0.171±0.087±0.028	−0.433±0.136±0.026
63.0	0.013±0.051±0.004	−0.211±0.074±0.016
89.0	0.152±0.034±0.011	−0.079±0.047±0.004
115.0	0.259±0.042±0.017	−0.172±0.055±0.012
141.0	0.258±0.056±0.021	−0.232±0.075±0.020
167.0	0.067±0.056±0.006	−0.172±0.080±0.014

model to the data, it is necessary to integrate over the bin size to obtain an average value equivalent to that for the data. In other words, the models were histogrammed into bins corresponding to the same bin sizes as the data. Each experimental point is counted as a degree of freedom and the comparison yields the results, listed in Table VII.

The results of the χ^2 comparison for the MAID, SL, and DMT models give very similar fits for the double-spin asymmetry A_{et}. The differences in the total χ^2 are primarily determined by the comparison with the single spin asymmetry A_t. On one hand, the double-spin asymmetry is characterized by the $|M_{1+}|^2$ term, which all the models describe reasonably well. The target asymmetry on the other hand involves the imaginary part of interference terms and therefore depends on multipoles such as E_{0+}, S_{0+}, M_{1+}, and S_{1-}, which have larger uncertainties in the models. In this respect, the SL model considers all the second order processes, whereas the MAID model makes approximations for these terms. A dynamic approach of DMT accounts for these

TABLE III. Asymmetries A_t and A_{et} as a function of center-of-mass angle of the pion $\cos\theta^*$ integrated over ϕ^* at low Q^2. The uncertainties listed are statistical and systematic, respectively. Please note that the results in this table are affected by the zero acceptance region (see Fig. 7).

	$0.5\ \mathrm{GeV}^2/c^2 < Q^2 < 0.9\ \mathrm{GeV}^2/c^2$	
	$0° < \phi^* < 180°$	$-180° < \phi^* < 180°$
$\cos\theta^*$	A_t	A_{et}
−0.938	−0.061±0.096±0.038	−0.045±0.135±0.008
−0.812	0.113±0.078±0.008	−0.336±0.119±0.044
−0.688	0.086±0.065±0.003	−0.170±0.093±0.015
−0.562	0.087±0.068±0.002	−0.165±0.097±0.014
−0.438	0.258±0.063±0.018	−0.244±0.084±0.021
−0.312	0.243±0.068±0.032	−0.139±0.089±0.012
−0.188	0.289±0.068±0.017	−0.145±0.088±0.011
−0.062	0.155±0.055±0.015	−0.298±0.080±0.017
0.062	0.262±0.051±0.013	−0.181±0.068±0.010
0.188	0.210±0.057±0.029	−0.114±0.077±0.006
0.312	0.200±0.047±0.011	−0.174±0.064±0.010
0.438	0.239±0.058±0.008	−0.172±0.077±0.010
0.562	0.146±0.058±0.014	−0.280±0.084±0.018
0.688	0.174±0.052±0.021	−0.178±0.072±0.012
0.812	0.110±0.058±0.004	−0.005±0.080±0.002
0.938	0.006±0.063±0.005	0.106±0.091±0.010

TABLE IV. Asymmetries A_t and A_{et} as a function of center-of-mass angle of the pion ϕ^* integrated over $\cos\theta^*$ at high Q^2. The uncertainties listed are statistical and systematic, respectively.

	$0.9\ \mathrm{GeV}^2/c^2 < Q^2 < 1.5\ \mathrm{GeV}^2/c^2$	
ϕ^* (deg)	A_t	A_{et}
−167.1	−0.056±0.129±0.004	−0.299±0.194±0.020
−141.4	−0.247±0.119±0.015	−0.178±0.160±0.012
−115.7	−0.250±0.096±0.015	−0.212±0.130±0.013
−90.0	−0.411±0.116±0.026	−0.146±0.136±0.011
−64.3	−0.504±0.162±0.053	−0.287±0.178±0.031
−38.6	−0.071±0.115±0.005	−0.070±0.162±0.006
−12.9	0.076±0.176±0.011	0.129±0.249±0.021
12.9	0.096±0.133±0.009	−0.325±0.202±0.033
38.6	−0.115±0.074±0.009	−0.271±0.107±0.020
64.3	0.095±0.067±0.006	−0.142±0.095±0.009
90.0	0.220±0.067±0.012	−0.156±0.090±0.009
115.7	0.189±0.067±0.011	−0.089±0.091±0.005
141.4	0.247±0.076±0.020	−0.179±0.101±0.014
167.1	0.295±0.089±0.015	−0.265±0.119±0.014

TABLE V. Asymmetries A_t and A_{et} as a function of center-of-mass angle of the pion $\cos\theta^*$ integrated over ϕ^* at high Q^2. The uncertainties listed are statistical and systematic, respectively.

	$0.9\ \mathrm{GeV}^2/c^2 < Q^2 < 1.5\ \mathrm{GeV}^2/c^2$	
	$0° < \phi^* < 180°$	$-180° < \phi^* < 180°$
$\cos\theta^*$	A_t	A_{et}
−0.929	0.281±0.271±0.002	0.322±0.366±0.096
−0.786	−0.100±0.120±0.008	−0.306±0.180±0.031
−0.643	−0.003±0.115±0.002	−0.512±0.196±0.049
−0.500	0.032±0.071±0.008	−0.203±0.103±0.016
−0.357	0.283±0.099±0.012	−0.420±0.141±0.029
−0.214	0.199±0.078±0.009	−0.212±0.107±0.011
−0.071	0.314±0.087±0.015	−0.154±0.112±0.007
0.071	0.279±0.081±0.009	−0.228±0.108±0.014
0.214	0.220±0.080±0.014	−0.171±0.109±0.008
0.357	0.228±0.094±0.019	−0.286±0.132±0.016
0.500	0.354±0.147±0.014	−0.135±0.176±0.011
0.643	0.158±0.075±0.008	−0.007±0.103±0.002
0.786	0.190±0.077±0.008	−0.113±0.105±0.007
0.929	0.390±0.169±0.008	0.239±0.203±0.025

TABLE VI. Asymmetries A_t and A_{et} as a function of the momentum transfer Q^2 integrated over ϕ^* and $\cos\theta^*$. The uncertainties listed are statistical and systematic, respectively.

	$-1<\cos\theta^*<1$	
	$0°<\phi^*<180°$	$-180°<\phi^*<180°$
Q^2 (GeV^2/c^2)	A_t	A_{et}
0.600	$0.171\pm0.019\pm0.014$	$-0.169\pm0.027\pm0.012$
0.800	$0.154\pm0.024\pm0.007$	$-0.146\pm0.033\pm0.010$
1.000	$0.205\pm0.036\pm0.008$	$-0.165\pm0.049\pm0.011$
1.200	$0.164\pm0.047\pm0.011$	$-0.207\pm0.066\pm0.012$
1.400	$0.223\pm0.059\pm0.017$	$-0.192\pm0.079\pm0.013$

second-order processes, but appears to give a similar fit as the MAID model. The effective Lagrangian model of DM does not include tails from higher resonances, limiting the background description even further, and may explain the large discrepancy with the polarization data.

The DMT and MAID models were also observed to give similar fits to each other for electron single spin A_e observed at lower Q^2 at JLab [22] and Mainz [21], although both are in somewhat disagreement with those data.

VI. SUMMARY

Target and double-spin asymmetries for the $\Delta(1232)$ region decaying into p and π^0 were extracted as a function of the pion center-of-mass angles θ^* and ϕ^* and the momentum transfer Q^2. A comparison with some of the existing theoretical approaches was performed and sensitivity to the different models was observed. A χ^2 comparison shows (see Table VII) that the model with the best agreement with data is the dynamical model of SL. The isobar model MAID and dynamic models of DMT exhibited comparable fits in reasonable agreement with the data. Keeping aside the speculations about the various model sensitivities given here, a discussion of the technical differences which give rise to the differences in theoretical approaches is beyond the scope of this paper. Rather, it is the intent of this work to make available the unique experimental observables as constraints on all the models mentioned in the Introduction.

TABLE VII. χ^2 per number of degree of freedom comparison between the data and the four theoretical models.

Model	A_t (ndf=102)	A_{et} (ndf=65)
MAID2000	1.8	1.1
SL	1.1	1.2
DM	4.1	1.7
DMT	2.0	0.9

ACKNOWLEDGMENTS

We thank R. M. Davidson, T. S. Lee, and L. Tiator for their valuable help. We acknowledge the efforts of the staff of the Accelerator and Physics Division at Jefferson Lab for making this experiment possible. This work was supported by the U.S. Department of Energy, the U.S. National Science Foundation, the French Commissariat a l'Energie Atomic, and the Italian Istituto Nazionale di Fisica Nucleare.

APPENDIX: MULTIPOLE NOTATION

The cross section for electroproduction in Eqs. (7) can also be written as a combination of Legendre polynomials and their first and second derivatives. The coefficients of this expansion are the multipoles: $E_{l\pm}$, $M_{l\pm}$, and $S_{l\pm}$ [36]. The multipoles characterize the excitation mechanism [electric (E), magnetic (M), and coulomb or scalar (S) type of photon] and the angular momentum of the final state πN. $l\pm$ refers to a state with a πN relative angular momentum l and total angular momentum $J=l\pm\frac{1}{2}$.

[1] D. Drechsel, O. Hanstein, S.S. Kamalov, and L. Tiator, Nucl. Phys. **A645**, 145 (1999).
[2] T. Sato and T.S. Lee, Phys. Rev. C **54**, 2660 (1996).
[3] S.S. Kamalov, G.Y. Chen, D. Drechsel, and L. Tiator, Phys. Lett. **B522**, 27 (2001).
[4] R.M. Davidson, N.C. Mukhopadhyay, and R.S. Wittman, Phys. Rev. D **43**, 71 (1991).
[5] T. Sato and T.S. Lee, Phys. Rev. C **63**, 055201 (2001).
[6] S. Kamalov and S.N. Yang, Phys. Rev. Lett. **83**, 4494 (1999).
[7] G. Knochlein, D. Drechsel, and L. Tiator, Z. Phys. A **352**, 327 (1995).
[8] I. Aznauryan and S. Stepanyan, Phys. Rev. D **59**, 54 009 (1999).
[9] R.A. Arndt, W.J. Briscoe, I.I. Strakovsky, and R.L. Workman, Proceedings of the Workshop on the Physics of Excited Nucleons (NSTAR2002) Pittsburgh, PA, USA, 2002 (unpublished), nucl-th/0301068.
[10] S. Capstick and B.D. Keister, Phys. Rev. D **51**, 3598 (1995).
[11] F. Cardarelli *et al.*, Phys. Lett. B **371**, 7 (1996).
[12] V.M. Belyaev and A.V. Radyushkin, Phys. Rev. D **53**, 6509 (1996).
[13] P. Stoler, Phys. Rev. D **65**, 053013 (2002).
[14] L.L. Frankfurt, V. Polyakov, M. Strikman, and M. Vanderhaeghen, Phys. Rev. Lett. **84**, 2589 (2000).
[15] C.E. Carlson and J.L. Poor, Phys. Rev. D **38**, 2758 (1988).
[16] G. Blanpied *et al.*, Phys. Rev. C **64**, 025203 (2001).
[17] R. Beck *et al.*, Phys. Rev. Lett. **78**, 606 (1997).
[18] F. Kalleicher *et al.*, Z. Phys. A **359**, 201 (1997).
[19] V.V. Frolov *et al.*, Phys. Rev. Lett. **82**, 45 (1999).
[20] K. Joo *et al.*, Phys. Rev. Lett. **88**, 122001 (2002).
[21] P. Bartsch, Phys. Rev. Lett. **88**, 142001 (2002).
[22] K. Joo *et al.*, nucl-ex/0301012.
[23] T. Pospischil *et al.*, Phys. Rev. Lett. **86**, 2959 (2001).
[24] C. Mertz *et al.*, Phys. Rev. Lett. **86**, 2963 (2001).

[25] R. De Vita *et al.*, CLAS Collaboration, Phys. Rev. Lett. **88**, 082001 (2002).
[26] D. Drechsel and L. Tiator, J. Phys. G **18**, 449 (1992).
[27] C. K. Sinclair, CEBAF Report No. CEBAF-PR-89-002.
[28] M. Borghini, CERN Report No. CERN-68-32 1968.
[29] A. Abragam, *The Principle of Nuclear Magnetism* (Clarendon, Oxford, 1961).
[30] C. Keith *et al.*, Nucl. Instrum. Methods Phys. Res. A **501**, 327 (2003).
[31] B. Mecking *et al.*, Nucl. Instrum. Methods Phys. Res. A **503**, 513 (2003).
[32] A. Biselli, Ph.D. thesis, Rensselaer Polytechnic Institute, 2002.
[33] T.W. Donnelly and A.S. Raskin, Ann. Phys. **169**, 247 (1986).
[34] M.K. Jones, Phys. Rev. Lett. **84**, 1398 (2000).
[35] L.W. Mo and Y.S. Tsai, Rev. Mod. Phys. **41**, 205 (1969).
[36] G.F. Chew, M.L. Goldberger, F.E. Low, and Y. Nambu, Phys. Rev. **106**, 1345 (1957).